

Penetration of High-Energy Electron Beams in Water*

NIKITAS D. KESSARIS

Division of Biophysics, Sloan-Kettering Institute for Cancer Research, New York, New York

(Received 24 June 1965; revised manuscript received 1 December 1965)

The penetration, scattering, and absorption of electron beams of energy 10 to 20 MeV in water has been mathematically investigated by solving the Lewis equation by the moment method under the continuous slowing-down approximation. Two beam geometries were considered: plane infinite monodirectional beam and point monodirectional beam, both incident on an infinite water medium. For the former, expressions were obtained for the flux, current, rate of energy deposition, rate of charge accumulation, and angular distribution as a function of depth, taking into account not only the incoming primary electrons, but also the contribution of the secondaries. For the latter geometry, expressions were obtained for the root-mean-square average of the flux and energy deposition as a function of depth.

I. INTRODUCTION

THE penetration, scattering and absorption of electron beams of energy 10 to 20 MeV in water is of great interest to biophysicists in attempting to understand the biological effects of radiation, as well as to radiologists in planning the irradiation of malignant tumors with minimal damage to adjacent tissue. Sources of such high-energy electron beams are the betatron and the linear accelerator, which have proved vital research tools to both biophysicists and radiologists in the last decade. These beams are nearly monochromatic. The finite electron mass gives the beams a well-defined finite maximum depth of penetration, as long as their initial energies are low enough to make bremsstrahlung losses a small part of the total losses. Knowledge of the rate of energy absorption, the beam spread, the spectrum, etc., in tissue-like matter is imperative in the proper utilization of such beams. From a basic standpoint, the problem has been mathematically explored under various simplifying assumptions, by various authors. The first quantitatively accurate solutions have been given in the case of low energies (below 1 MeV) for a single quantity, namely, the rate of energy dissipation.¹ Adawi² calculated this quantity also for higher energies on the basis of the first three moments. Spencer¹ extended his calculations up to 10 MeV for some low atomic number elements and for air and polystyrene, but not water. Transmission curves in carbon and aluminum have been obtained by Leiss *et al.*³ and Perkins⁴ by Monte Carlo methods. Our objective is not only to expand the scope of the problem by deriving a wide variety of physically meaningful quantities, but also to treat it in its entirety, so as to include brems-

strahlung production. However, the continuous slowing-down approximation is retained throughout our treatment. The pencil beam geometry has been previously explored by Crew⁵ using the moment method for 0.4-MeV electrons in air, and recently by Berger⁶ using the Monte Carlo method for electrons up to 10 MeV in water.

II. THE BEAM GEOMETRIES

Two beam geometries will be investigated: the infinite monodirectional plane beam and the point-monodirectional beam. Both beams are monoenergetic, and they are embedded in a medium (water) of infinite extent. The problem can be generalized to include beams of any directional or spectral characteristics by linear superposition of our solutions. The limitation to an infinite medium enables one to solve the transport equation by the moment method, as it is done in this paper. For a medium whose thickness is much smaller than the total track length, the problem is solved (approximately) by invoking the small-angle small-depth approximation. Monte-Carlo solutions are also possible for the above cases as well as others: for example, for the case where the thickness is neither very small nor very large.

III. THE TRANSPORT EQUATION

The equation pertinent to the problem of electron penetration is

$$-\frac{\partial I(\mathbf{r}, R, \boldsymbol{\Omega})}{\partial R} + \nabla \cdot (\boldsymbol{\Omega} I) = \int d\Omega' \sigma_{\text{Ruth}}(R, \Theta) \times [I(\mathbf{r}, R, \boldsymbol{\Omega}') - I(\mathbf{r}, R, \boldsymbol{\Omega})] + Q(\mathbf{r}, R, \boldsymbol{\Omega}), \quad (1)$$

which is sometimes known as the Lewis equation. This equation is simply a continuity equation in the phase-space element $d\tau = dV(d\Omega dR)$ for the angular number flux $I(\mathbf{r}, R, \boldsymbol{\Omega})$. $I(\mathbf{r}, R, \boldsymbol{\Omega})$ is defined so that $I d\Omega dR$ is the number of electrons of residual range between R and $R+dR$ moving in the direction of the unit vector $\boldsymbol{\Omega}$ in the element of solid angle $d\Omega$ and crossing (per unit

* This paper contains portions of a thesis to be submitted by the author in partial fulfillment of the requirements for the degree of Doctor of Philosophy in the Faculty of the Physics Department, Harvard University. This work was supported in part by U. S. Atomic Energy Commission Contract AT(30-1)910. The computer work on the IBM 7090 was supported by U. S. Public Health Service Research Grant No. CA-06102.

¹ L. V. Spencer, *Phys. Rev.* **98**, 1597 (1955); *Natl. Bur. Std. (U. S.) Monograph No. 1* (1959).

² I. Adawi, *Phys. Rev.* **107**, 1476 (1957).

³ J. E. Leiss, S. Penner, and C. S. Robinson, *Phys. Rev.* **107**, 1544 (1957).

⁴ J. F. Perkins, *Phys. Rev.* **126**, 1781 (1962).

⁵ J. E. Crew, *J. Res. Natl. Bur. Std.* **65A**, No. 2 (1961).

⁶ M. J. Berger, National Bureau of Standards Report No. 8678, 1965 (unpublished).

time) a unit area normal to Ω at the point \mathbf{r} . The quantity σ_{Ruth} is a Rutherford-type cross section and $Q(\mathbf{r}, R, \Omega)$ is the source term.

Equation (1) is based on the continuous slowing-down approximation. This approximation arises from an examination of the energy losses suffered by the incoming electron in colliding with electrons and nuclei in the medium. The cross section for electron-electron collisions is proportional to q^{-2} , where q is the fractional energy loss,⁷ so it is weighed heavily toward very small energy losses. These losses are then treated as continuous rather than discrete and a function (the stopping power) can be defined which gives the rate of energy loss with track length.⁸⁻¹¹ This assumption will be examined further in the section on secondary electron distributions. The continuous slowing-down assumption is applicable to interactions resulting in excitation or ionization, not to interactions resulting in production of bremsstrahlung, in which case photons of large fractional energies can be produced. For an incoming electron of 20-MeV energy, a total of 1.6 MeV of its energy goes into bremsstrahlung. For 15- and 10-MeV electrons, the amounts are 0.9 and 0.4 MeV, respectively (in water). Although photons with an energy up to the electron energy can be produced, the spectrum is weighted toward soft photons. It was then decided to consider the average rate of energy loss by bremsstrahlung,¹² which was then added to the rate of ionization loss. In the section on the rate of energy absorption we will obtain the rate of photon production and absorption, and we will see to what extent bremsstrahlung losses modify the results based on the continuous slowing down approximation. From the total stopping power we obtain the average track length $R(T)$ that an electron of energy T will traverse. We next consider the angular deflections due to nuclear, electron, and bremsstrahlung scattering. The relativistically correct nuclear scattering cross section must be modified to include: (1) the effect of screening of the nuclear field by orbital electrons, (2) inelastic electron-electron scattering, and (3) deflection due to production of bremsstrahlung.

The cross section that takes into account the first two effects is the McKinley-Feshback cross section¹³:

$$2\pi\sigma(\beta, \vartheta) = \frac{\pi r_0^2}{2\beta^4} Z(Z+1)(1-\beta^2) \left(\sin^2 \frac{\vartheta}{2} + \eta^2 \right)^{-2} \times \left[1 - \beta^2 \sin^2 \frac{\vartheta}{2} + \frac{\pi\beta Z}{137} \sin \frac{\vartheta}{2} \left(1 - \sin \frac{\vartheta}{2} \right) \right], \quad (2)$$

⁷ W. Heitler, *Quantum Theory of Radiation* (Oxford University Press, Oxford, England, 1954), 3rd ed., p. 240.

⁸ E. Fermi, *Nuclear Physics* (University of Chicago Press, Chicago, Illinois, 1951), revised ed., p. 28.

⁹ R. M. Sternheimer, *Phys. Rev.* **103**, 511 (1956).

¹⁰ F. W. Spiers, in *Radiation Dosimetry*, edited by G. Hine and G. L. Brownell (Academic Press Inc., New York, 1956), p. 27.

¹¹ In the formula for the rate of energy loss (stopping power) the quantity I , the average ionization potential of the medium, appears. In this work the value $I=78$ eV for water was used.

¹² W. Heitler, *Ref. 7*, p. 251.

¹³ W. A. McKinley and H. Feshback, *Phys. Rev.* **74**, 1759 (1948).

where Z is the atomic number of the medium, T is the kinetic energy of the electron in m_0c^2 units, r_0 is the classical electron radius, and η is the screening angle^{14,15} for which Adawi's expression² will be adopted here. Accurate experimental data on such quantities as the transmission function, and the flux of electrons may indicate the extent to which this choice has to be modified.

The effect of bremsstrahlung angular scattering is about two orders of magnitude less than that of Rutherford scattering.¹⁶ Its inclusion involves enormous theoretical and computational complications, and was thus omitted.

A pilot calculation, based on results of Brysk,¹⁷ showed that, for the beam energies under consideration, the flux of bremsstrahlung secondaries was less than 5% of the flux of Moller-collision secondaries and less than 1% of the primary flux. Consequently, in subsequent calculations, the bremsstrahlung secondaries were ignored.

IV. THE PLANE INFINITE BEAM

Basic Considerations

The geometry of the source indicates that we should use cylindrical coordinates for the space variables and spherical polar coordinates to specify the direction of the momentum. The energy is specified by the residual range, $R(E)$. Cylindrical symmetry considerations and the infinite extent of the beam, reduce the space variables to one, namely, the depth z , and the momentum angular variables also to one, namely, the angle that the particle makes with the z axis. Then Eq. (1) becomes:

$$-\frac{\partial I(z, R, \vartheta)}{\partial R} + \cos \vartheta \frac{\partial I(z, R, \vartheta)}{\partial z} = \int d\Omega' N \sigma(R, \Theta) [I(z, R, \vartheta') - I(z, R, \vartheta)] + \frac{\delta(1 - \cos \vartheta) \delta(z) \delta(R - R_0)}{2\pi}, \quad (3)$$

where Θ , the angle between the directions Ω , Ω' , is given by

$$\cos \Theta = \Omega \cdot \Omega' = \cos \vartheta \cos \vartheta' + \sin \vartheta \sin \vartheta' \cos(\phi - \phi'),$$

and

$$d\Omega = \sin \vartheta d\vartheta d\phi.$$

¹⁴ N. Bethe, *Phys. Rev.* **89**, 1256 (1953).

¹⁵ G. Moliere, *Z. Naturforsch.* **3a**, 78 (1948).

¹⁶ M. Stearns, *Phys. Rev.* **76**, 836 (1949); L. I. Schiff, *ibid.* **83**, 252 (1951).

¹⁷ H. Brysk, *Phys. Rev.* **96**, 419 (1954); D. T. Goldman and H. Brysk, *Am. J. Roentgenol., Radium Therapy Nucl. Med.* **74**, 323 (1955).

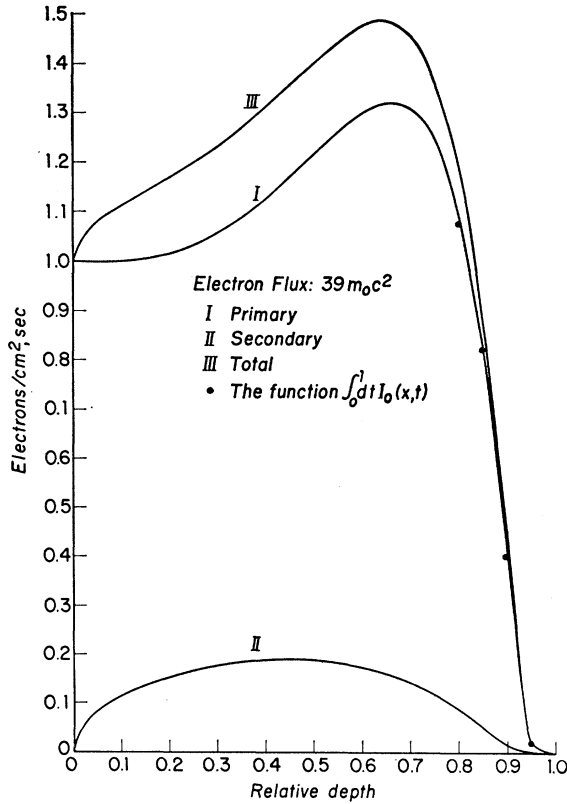


FIG. 1. The flux distribution as a function of relative depth $x = z/R_0$. The total flux, curve III, is the sum of the primary flux, curve I, and the secondary flux, curve II.

R_0 is the residual range that corresponds to the initial energy, E_0 . Both z and R are expressed in units of g/cm^2 . The distribution function, then, has dimensions of electrons per unit solid angle, per unit residual range per cm^2 per sec. N is the number of atoms per gram.

Following the procedure of Ref. 1, we redefine our variables z and R as follows:

$$z = R_0 x, \quad R = R_0 t. \quad (4)$$

Defining

$$I_{ln}(t) = 2\pi \int_0^\pi P_l(\cos\vartheta) \sin\vartheta d\vartheta \int_{-1}^1 x^n I(x, t, \vartheta) dx, \quad (5)$$

we arrive at the equations for $I_{ln}(t)$:

$$\begin{aligned} -\frac{\partial I_{ln}(t)}{\partial t} + S_l(t) I_{ln}(t) \\ = \frac{n}{2l+1} [(l+1) I_{l+1, n-1}(t) + l I_{l-1, n-1}(t)] \\ + \delta_{n0} \delta(1-t), \quad (6) \end{aligned}$$

where $S_l(t)$ is given in Ref. 2, Eq. (3), and else-

where.^{1,18,19} The solution of Eq. (6) is

$$I_{l0}(t) = \exp \left\{ - \int_t^1 dt' S_l(t') \right\}, \quad (7)$$

$$\begin{aligned} I_{ln}(t) = n(2l+1)^{-1} I_{l0}(t) \int_t^1 [I_{l0}(t')]^{-1} \\ \times [(l+1) I_{l+1, n-1}(t') + l I_{l-1, n-1}(t')] dt'. \quad (8) \end{aligned}$$

Setting $\cos\vartheta = 1$ in Eq. (3) (small-angle case), approximately $S_l(t)$ by

$$S_l(t) = Al(l+1)t^{-2}, \quad (9)$$

and applying the Laplace operator

$$\int_{-\infty}^{1-t} dx \exp\{p(x+t-1)\},$$

we arrive at

$$\begin{aligned} I(x, t, \vartheta) = (2\pi)^{-1} (2Ax)^{-1} \delta(1-t-x) \\ \times \exp\{-(1-x)(4Ax)^{-1} \vartheta^2\}, \quad (10) \end{aligned}$$

from which

$$\langle \vartheta^2 \rangle_{av} = 4Ax(1-x)^{-1}. \quad (11)$$

Equation (10) requires that

$$t+x=1, \quad \text{or} \quad x=1-t. \quad (12)$$

Lifting the small-angle condition, we have the general case

$$t+x \leq 1, \quad \text{or} \quad x \leq 1-t, \quad (13)$$

which we propose to investigate.

The Primary Distribution

We find the following quantities:

(1) The flux as a function of depth:

$$I_0(x) = \int_0^1 dt \int_0^\pi \sin\vartheta d\vartheta I(x, t, \vartheta) \equiv \int_0^1 dt I_0(x, t). \quad (14)$$

(2) The current in the x direction as a function of depth:

$$I_1(x) = \int_0^1 dt \int_0^\pi \sin\vartheta d\vartheta \cos\vartheta I(x, t, \vartheta) \equiv \int_0^1 dt I_1(x, t). \quad (15)$$

(3) The rate of charge accumulation as a function of depth:

$$Q(x) = -dI_1(x)/dx. \quad (16)$$

(4) The rate of energy absorption, i.e., the energy per unit depth, per gram absorbed at a depth x .

¹⁸ G. Goudsmit and J. L. Saunderson, Phys. Rev. **57**, 24 (1940); **58**, 36 (1940).

¹⁹ H. W. Lewis, Phys. Rev. **98**, 1597 (1955).

TABLE I. Values for the parameters of $I_0(x)$, $I_1(x)$.

	T_0	a^2	A_1	A_2	A_3	A_4	A_5
$I_0(x)$	$39m_0c^2$	0.253	0.253	0.285	3.06	0	0
	$30m_0c^2$	0.322	0.322	0.374	4.115	0	0
	$20m_0c^2$	0.462	0.462	0.569	6.63	0	0
$I_1(x)$	$39m_0c^2$	0.295	0.295	0.3385	0.386	0.439	0.468
	$30m_0c^2$	0.340	0.340	0.398	0.462	0.534	0.201
	$20m_0c^2$	0.410	0.410	0.494	0.590	0.135	0

(5) The average angular distribution:

$$\langle 1 - \cos\vartheta \rangle_{av} = [I_0(x) - I_1(x)] / I_0(x) \quad (17)$$

as a function of depth.

(6) The average statistical relationship between depth and track length:

$$\langle x \rangle_{av} = I_{01}(t) / I_{00}(t). \quad (18)$$

(7) The energy, or track length spectrum.

(8) The energy spectrum at various depths. The quantities (1) to (5) will be found from their moments (with respect to x) and the appropriate B.C.'s and their behavior at $(1-x) \ll 1$.

The moments of $I_l(x)$, $l=0, 1, 2$, etc., are

$$i_{ln} = \int_0^1 dt I_{ln}(t) = \int_{-1}^1 dx x^n I_l(x), \quad (19)$$

and can thus be immediately calculated from the $I_{ln}(t)$ which were themselves numerically calculated for all l, n such that

$$l+n \leq 10.$$

The B.C. at $x=0$ is

$$I_l(0+) - I_l(0-) = 1 \quad (20)$$

which under the assumption (to be validated later)

$$I_l(x) = 0, \quad x < 0, \quad (21)$$

becomes

$$I_l(0+) = 1. \quad (22)$$

The behavior at large depths has been shown by Wick²⁰ (in the case of neutron penetration) and Spencer¹ (who adapted Wick's treatment to electrons) to be

$$I_l(x) \sim \exp\{-a^2 x(1-x)^{-1}\}. \quad (23)$$

Among the various methods of solution, the function-fitting method proved to be the only fruitful one. A simplified function-fitting solution, not making use of the Gauss technique,²¹ gave a fit to the prescribed moments with an accuracy of better than 1%, and had the correct initial and large depth behavior. For $I_0(x)$ and $I_1(x)$ the function was

$$I(x) = \left(\sum_{j=0}^s A_j x^j \right) \exp\{-a^2 x(1-x)^{-1}\} \quad (24)$$

²⁰ G. C. Wick, Phys. Rev. 75, 738 (1949).

²¹ L. V. Spencer and U. Fano, J. Res. Natl. Bur. Std. 46, 446 (1951); L. V. Spencer, Phys. Rev. 88, 793 (1952).

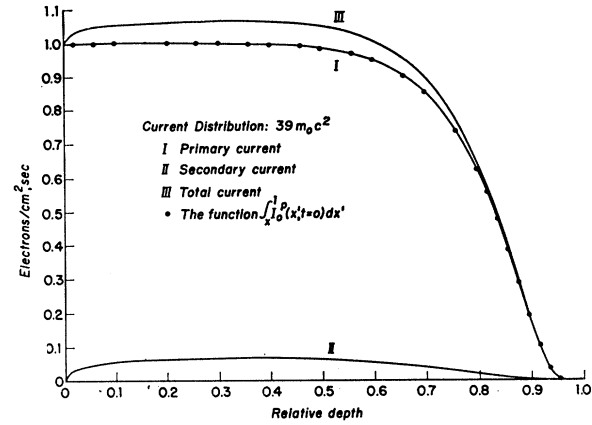


FIG. 2. The current distribution as a function of relative depth $x=R_0$. The total current, curve III, is the sum of the primary current, curve I, and the secondary current, curve II.

with $A_0=1$. The values of a^2 , A_j are given in Table I, and $I_0(x)$, $I_1(x)$ are plotted in Figs. 1 and 2, curve I, respectively, for $T_0=39m_0c^2$. The rate of charge accumulation, Eq. (15), is readily obtained from $I_1(x)$ and plotted in Fig. 3, curve I. This curve, as well as those for $I_0(x)$, $I_1(x)$, will be considerably changed with the inclusion of the contribution of the secondary electrons.

The remarkable accuracy with which the moments and the boundary conditions can be fitted by the simple expression, Eq. (24), which ignores back scattering into the region $x < 0$ indicates that back scattering is indeed negligible. If the assumption of Eq. (21) is dropped and a back-scattering term (of the form $Be^{b\pi/(1+x)}$, for example) is included in the trial function, for best fit this term must be extremely small. The back-scattered component is likewise negligibly small for all the rest of the primary-electron distributions that we will investigate.

A function constructed from a finite number of moments can, of course, be realized in many ways, with, possibly, different results. Thus, a cross check on our results is most desirable. Such an opportunity is afforded by the distribution $I_0(x, t)$ (see below) from which the functions $I_1(x)$, $Q(x)$, and $I_0(x)$ can be obtained independently and compared to the results above. Such a comparison is shown in Figs. 1, 2, and 3. Agreement is very good.

The rate of energy absorption with depth, which finds important applications in radiobiology and radiotherapy, was also obtained. The details of the calculation and the results are reported elsewhere.²² This was done by calculating the rate of total energy dissipation, subtracting from it the rate of bremsstrahlung production, correcting the result for the finite range of knock-on secondaries, and adding to the result the rate of bremsstrahlung absorption.

²² N. D. Kessaris, Radiation Res. 23, 630 (1964).

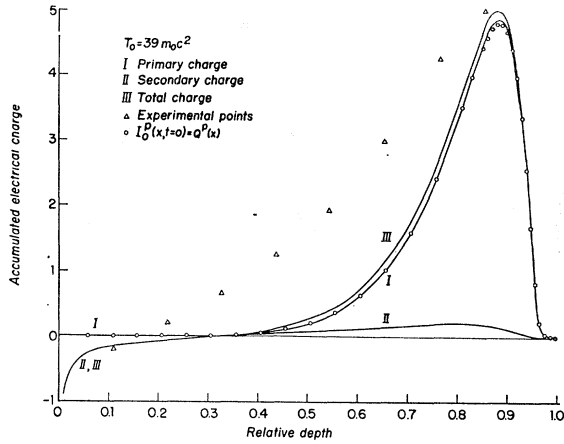


FIG. 3. The rate of charge accumulation as a function of relative depth, $x = z/R_0$. The total rate, curve III, which is the sum of the primary rate, curve I, and the secondary rate, curve II, is seen to become negative for small depths. Experimental points are also shown (see Ref. 20).

The quantity

$$\langle 1 - \cos\vartheta \rangle_{av}$$

has been obtained directly from the moments of $[I_0(x) - I_1(x)]$ rather by subtracting $I_1(x)$ from $I_0(x)$, both of which have already been obtained. This was done because any small errors in the fit of $I_0(x)$ or $I_1(x)$ are magnified many times, especially near $x = 0$ where they are both nearly unity and also near $x = 1$ where they decay very fast. The moments $(i_{0n} - i_{1n})$ were plotted on large semilogarithmic paper as a function of $(n+2)^{1/2}$. The result was as perfect a straight line as the plotting of the points permitted. This means that they are given by the expression

$$i_{0n} - i_{1n} = B \exp\{-2d(n+2)^{1/2}\}.$$

We can then show that $[I_0(x) - I_1(x)]$ is given by

$$[I_0(x) - I_1(x)] = Bd\pi^{-1/2}x(-\ln x)^{-3/2} \exp\{d^2/\ln x\}. \quad (25)$$

The decay constant is determined from $i_{0n} - i_{1n}$, $n \gg 1$. B is found from

$$i_{00} - i_{10} = B \exp\{-2^{3/2}d\}.$$

The parameters d^2 , B are given in Table II. The quantity goes to zero as $x \rightarrow 1$. This is so because the particles that have arrived near $x = 1$ must have traveled

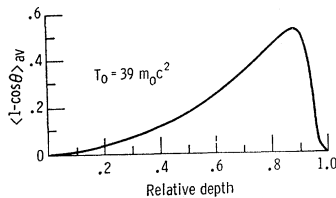


FIG. 4. The average angular distribution, $\langle 1 - \cos\vartheta \rangle_{av}$, as a function of the relative depth $x = z/R_0$.

TABLE II. Parameters of the distribution $[I_0(x) - I_1(x)]$.

T_0	$39m_0c^2$	$30m_0c^2$	$20m_0c^2$
B	1.262	1.671	2.547
d^2	0.436	0.517	0.666

in a nearly straight line, so that

$$\langle \cos\vartheta \rangle_{av} \simeq 1 \quad \text{or} \quad \langle 1 - \cos\vartheta \rangle_{av} \simeq 0, \quad x \simeq 1.$$

The magnitude of the maximum increases and the depth at which it occurs decreases as the beam energy decreases, as it is expected on physical grounds. Plots of $\langle 1 - \cos\vartheta \rangle_{av}$ are given in Fig. 4, for $T_0 = 39m_0c^2$.

The average depth that an electron with a residual range t has reached is given by Eq. (18). It is seen from Fig. 5 ($T_0 = 39m_0c^2$) that for most values of t , we have $\langle x \rangle_{av} \simeq 1 - t$.

The distribution of $I_0(x, t)$ was constructed from its moments, the $I_{0n}(t)$. On plotting $(1-t)^{-n}I_{0n}(t)$ for any t , against $(n+1+A)^{1/2}$ on semilog paper, a straight line was obtained (with an accuracy of $\frac{1}{2}\%$ or less) when A was suitably chosen. The resulting distribution is thus

$$I_0(x, t) = \pi^{-1/2}d \exp\{2d(1+A)^{1/2}\} (1-t)^{-1-A} \times x^A (-\ln x/1-t)^{-3/2} \exp\left\{\frac{d^2}{\ln x/1-t}\right\}. \quad (26)$$

The parameters A , d as functions of t are given in Fig. 6. The energy spectrum $I_0(x, T)$ is given by

$$I_0(x, T) = I_0(x, t)[dT/dt]^{-1}. \quad (27)$$

Samples of such spectra appear in Fig. 7 for an incident beam of energy $T_0 = 39m_0c^2$. A sample of moments appears in Table III.

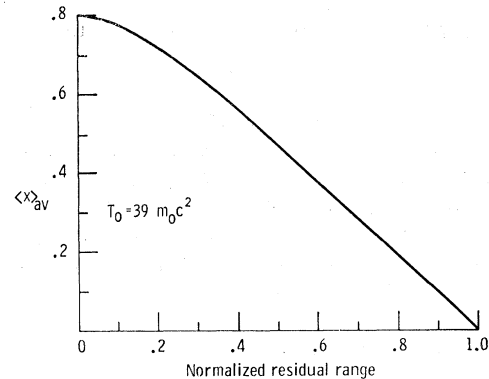


FIG. 5. The average penetration depth $\langle x \rangle_{av}$ as a function of the normalized residual track-length, $t = R/R_0$. It is seen that for most of the range of t , we have $\langle x \rangle_{av} \simeq 1 - t$.

TABLE III. Sample of the moments of $I_0^p(x, t)$ (round off to four significant figures).

n	$T_0=39m_0c^2$		$(1-t)^{-n}I_{0n}^p(t)$		$T_0=20m_0c^2$	
	$t=0$	$t=0.1$	$t=0$	$t=0.1$	$t=0$	$t=0.1$
0	1.000	1.000	1.000	1.000	1.000	1.000
1	0.8048	0.8648	0.7815	0.8223	0.7378	0.8000
2	0.6591	0.7574	0.6247	0.7217	0.5638	0.6581
3	0.5468	0.6695	0.5073	0.6257	0.4401	0.5504
4	0.4584	0.5964	0.4172	0.5477	0.3499	0.4671
5	0.3878	0.5348	0.3467	0.4833	0.2821	0.4007
6	0.3309	0.4826	0.2910	0.4298	0.2304	0.3475
7	0.2846	0.4384	0.2466	0.3851	0.1903	0.3042
8	0.2467	0.3994	0.2107	0.3477	0.1590	0.2679
9	0.2146	0.3665	0.1807	0.3145	0.1340	0.2370
10	0.1881	0.3360	0.1562	0.2863	0.1135	0.2121

From Eqs. (7) and (8) we have for the case $l=0$:

$$I_{0n}(t=0) = n \int_0^1 I_{1,n-1}(t') dt' + \delta_{n0} = ni_{1,n-1} + \delta_{n0}.$$

On the other hand,

$$\begin{aligned} \int_0^1 Q(x)x^n dx &= - \int_0^1 \frac{dI_1(x)}{dx} x^n dx \\ &= n \int_0^1 I_1(x)x^{n-1} dx - x^n I_1(x) \Big|_0^1 = ni_{1,n-1} + \delta_{n0}. \end{aligned}$$

Consequently,

$$\int_0^1 I_0(x, t=0)x^n dx = \int_0^1 Q(x)x^n dx$$

for all integral values of n such that $n \geq 0$. Thus,

$$I_0(x, t=0) = Q(x).$$

Integrating this expression from x to 1 we derive

$$\int_x^1 I_0(x', t=0) dx' = I_1(x).$$

The function $I_0(x)$ can also be derived from $I_0(x, t)$

$$I_0(x) = \int_0^1 I_0(x, t) dt.$$

Values of $I_0(x)$, $I_1(x)$, $Q(x)$ obtained from $I_0(x, t)$ are shown in Figs. 1, 2, and 3.

The Secondary Distribution

The integrodifferential equation obeyed by the secondary electrons has already been quoted in its general form in Sec. III, Eq. (1). In the case of an infinite beam and an infinite medium, it reduces to

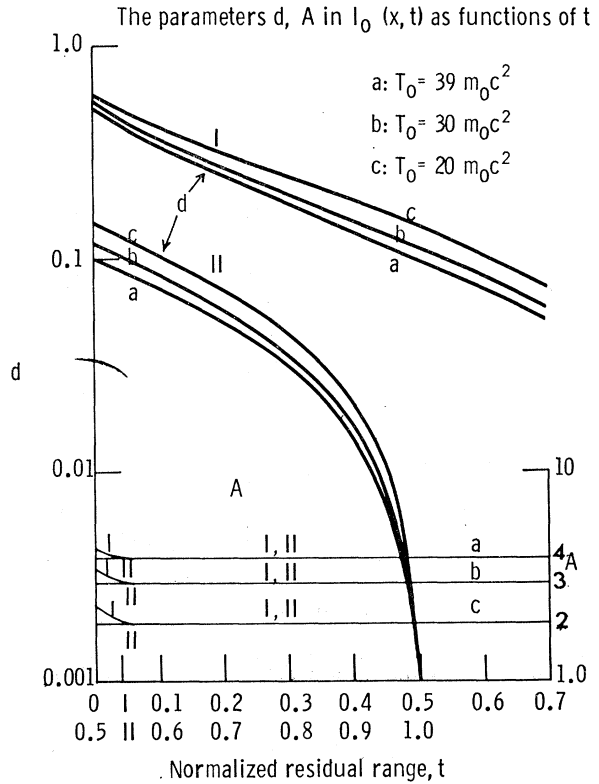


FIG. 6. The parameters d, A , which appear in $I_0(x, t)$, Eq. (26), the path-length distribution at depth x .

Eq. (3), with the source term replaced by

$$(2\pi)^{-1} \int_{4\pi} d\Omega' \int_{R(2T)}^{R_0} dR' N_e p(R, R') \times \delta[\mu - \mu(R, R')] I^p(z, R', \Omega'), \quad (28)$$

where $p(R, R')$ is the cross section of the production of a secondary with a residual range between R and $R+dR$ by a primary of residual range R' . It is related to the Møller cross section by

$$p(R, R') dR = \sigma_{M\ddot{o}ller}(T, T') dT.$$

Also^{7,23}

$$\mu(R, R') = [T(T'+2)/T'(T+2)]^{1/2},$$

where T is the kinetic energy of the secondary and T' that of the primary in m_0c^2 units. $\sigma_{M\ddot{o}ller}$ is given by

$$\sigma_{M\ddot{o}ller} = 2\pi r_0^2 \beta^{-2} [T^{-2} - (2T'+1)(T'+1)^{-2} T^{-1}(T'-T) + (T'-T)^{-2} + (T'+1)^{-2}]. \quad (29)$$

The Møller formula has been shown to be valid for energies up to 100 MeV.²⁴

²³ C. Møller, Ann. Physik 14, 531 (1932).

²⁴ E. B. Dally, Phys. Rev. 123, 1840 (1961).

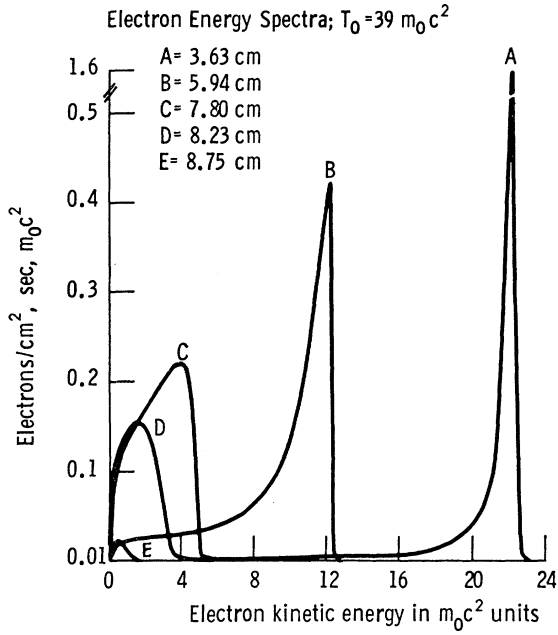


FIG. 7. The energy spectrum of electrons at various indicated depths of penetration. The initial electron energy is $39m_0c^2$.

In the reduced variables x, t the equation is then

$$\left[-\frac{\partial}{\partial t} + \cos\vartheta \frac{\partial}{\partial x} \right] I^s(x, t, \vartheta) = \int_{4\pi} d\Omega' S(t, \Theta) [I^s(x, t, \vartheta') - I^s(x, t, \vartheta)] + (2\pi)^{-1} \int_{4\pi} d\Omega' \int_{t(2T)}^1 dt' G(t, t') \delta[\mu - \mu(t, t')] \times I^p(x, t, \vartheta'), \quad (30)$$

where

$$G(t, t') = N_e R_0 S(t) \sigma_{M\ddot{o}ller} [T(t), T'(t)]. \quad (31)$$

All the other quantities have been defined previously. The equation for the Legendre-Moment coefficients is

$$\left[-\frac{\partial}{\partial t} + S_l(t) \right] I_{ln}^s(t) = n(2l+1)^{-1} \times [(l+1)I_{l+1, n-1}^s(t) + lI_{l-1, n-1}^s(t)] + R_{ln}(t), \quad (32)$$

which has the solution

$$I_{ln}^s(t) = I_{l0}^p(t) \int_t^{t(T_0/2)} dt' [I_{l0}^p(t')]^{-1} \times \left\{ \frac{n}{2l+1} [(l+1)I_{l+1, n-1}^s + lI_{l-1, n-1}^s] + R_{ln}(t') \right\}. \quad (33)$$

The quantities $R_{ln}(t)$ are given by

$$R_{ln}(t) = \int_{t(2T)}^1 dt' G(t, t') P_l[\mu(t, t')] I_{ln}^p(t'). \quad (34)$$

Finally, the moments are obtained by integration

$$i_{ln}^s = \int_0^1 dt I_{ln}^s(t). \quad (35)$$

Actual numerical calculation of the $I_{ln}^s(t)$ shows that they are extremely small at the highest energies (highest t 's) and rapidly increase with decreasing t . A comparison of the spectrum of secondaries, $I_{00}^s(t)$, against the primary spectrum, $I_{00}^p(t)$, gives a quantitative estimate of the validity of the continuous slowing-down approximation: the 10% point [$I_{00}^s(t)/I_{00}^p(t) = 0.1$] is reached for $t = 0.17$ for the $39m_0c^2$ beam and $t = 0.160$ for the $20m_0c^2$ case. The 100% point corresponds to values of t between 0.0076 and 0.011 (Fig. 8). The average over-all ranges of the secondaries as calculated from

$$\langle t \rangle_{av} = \int_0^1 dt t I_{00}^s(t) / \int_0^1 dt I_{00}^s(t)$$

are $\langle t \rangle_{av} = 0.0474, 0.0485, 0.0506$ for the 39, 30, and $20m_0c^2$ beams, respectively.

Comparing the relative magnitudes of $I_{00}^s(t)$ to $I_{10}^s(t)$ and, in general, to $I_{l0}^s(t)$, we see that the secondaries are produced strongly in the forward direction, although this trend is not as strong as that of the primary electrons. Consequently, backscattering is expected to be small.

The magnitude of moments i_{ln}^s is at least an order of magnitude less than the i_{ln}^p so their contribution to the flux, current, etc., will be correspondingly small. This validates the perturbation-iteration procedure employed to find the secondary electron distribution.

The moments $i_{0n}^s, i_{1n}^s, i_{1n}^{1s}$, where

$$i_{1n}^{1s} = \int_0^1 dt I_{1n}^s(t) dt$$

were carefully plotted and their asymptotic trend for $n \gg 1$ was examined. They were plotted on semilog paper against $(n+A)^{1/2}$, where A was adjusted to give a linear trend. In addition, the tentative omission of backscattering imposes the condition that all functions,

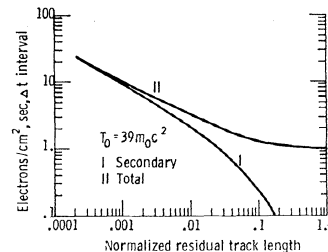


FIG. 8. The electron spectrum as a function of the normalized residual track length, $t = R/R_0$.

TABLE IV. Values of the parameters of $I_0^s(x)$, $I_1^s(x)$, $I_1^{1s}(x)$, $\langle t \cos\vartheta \rangle_{av}^s$.

		$I_0^s(x)$	$I_1^s(x)$	$I_1^{1s}(x)$	$\langle t \cos\vartheta \rangle_{av}^s$
$39m_0c^2$	A	0.375	0.124	0.0199	0.0532
	α	1/2	1/3	1/2	0
	a^2	0.34	0.42	0.93	0.59
$30m_0c^2$	A	0.373	0.125	0.0201	0.0540
	α	1/2	0.40	1/2	0
	a^2	0.41	0.50	1.10	0.69
$20m_0c^2$	A	0.386	0.110	0.0195	0.0504
	α	16/30	13/30	16/30	0
	a^2	0.54	0.64	1.28	0.74

$I_0^s(x)$, $I_1^s(x)$, etc., are zero at $x=0$, so their behavior near $x=0$ is as a positive power of x : x^α . Under the same assumption it can be shown that $\alpha < 1$.

It was then found that the moments of the secondary flux, current, etc., together with their initial and asymptotic behavior, can be fitted by the following simple expression:

$$Ax^\alpha \exp\{-a^2x(1-x)^{-1}\}.$$

The appropriate values of A , α , a^2 are given in Table IV.

The total flux, current and charge are simply

$$I_0^p(x) + I_0^s(x), \quad I_1^p(x) + I_1^s(x), \\ Q^p(x) + Q^s(x) = -(d/dx)[I_1^p(x) + I_1^s(x)],$$

respectively. The rate of secondary charge accumulation

$$\left[-\frac{\partial}{\partial t} + \cos\vartheta \frac{\partial}{\partial x} + \sin\vartheta \cos\Phi \frac{\partial}{\partial \rho} - \rho^{-1} \sin\vartheta \sin\Phi \frac{\partial}{\partial \Phi} \right] I(\rho, \vartheta, x, t, \Phi) \\ = \int d\Omega' S(t, \Theta) [I(\rho, \vartheta', x, t, \Phi') - I(\rho, \vartheta, x, t, \Phi)] + (2\pi)^{-1} \rho^{-1} \delta(\rho) \delta(1 - \cos\vartheta) \delta(x) \delta(1 - t), \quad (36)$$

where

$$I(\rho, \vartheta, x, t, \Phi) = R_0^3 I(r, \vartheta, z, R, \Phi), \quad S(t, \Theta) = R_0 S(R, \Theta).$$

Applying the operator

$$L = \int_0^1 \rho^p d\rho \int_{-1}^1 x^n dx \int_0^{2\pi} \exp(im\Phi) d\Phi \int_0^\pi P_{lm}(\cos\vartheta) \sin\vartheta d\vartheta$$

to Eq. (36), and defining

$$LI(\rho, \vartheta, x, t, \Phi) = I_{l,m}^{n,p}(t),$$

there result the equations for $I_{l,m}^{n,p}(t)$:

$$[-(\partial/\partial t) + S_l(t)] I_{l,m}^{n,p}(t) = n(2l+1)^{-1} [(l-m+1)I_{l+1,m}^{n-1,p}(t) + (l+m)I_{l-1,m}^{n-1,p}(t)] \\ + (4l+2)^{-1}(p+m) [(l-m+1)(l-m+2)I_{l+1,m-1}^{n,p-1}(t) - (l+m-1)(l+m)I_{l-1,m-1}^{n,p-1}(t)] \\ - (4l+2)^{-1}(p-m) [I_{l+1,m+1}^{n,p-1}(t) - I_{l-1,m+1}^{n,p-1}(t)] + \delta_p \delta_n \delta_m \delta(1-t), \quad (37)$$

where $S_l(t)$ is already defined. Here $m = -p, -p+2, -p+4, \dots, p-4, p-2, p$ and $l \geq |m|$. The $I_{l,m}^{n,p}(t)$ were obtained for all values of l, n, p such that

$$l+n+p \leq 10, \quad p \leq 4.$$

becomes negative, for small values of x . This means that charge is knocked out of this region into a region of greater depth. So for $x \ll 1$ we have a region of positive charge. This actually has been confirmed experimentally.

The quantity $I_1^{1s}(x)$ was constructed in order to obtain $\langle t \cos\vartheta \rangle_{av}^s$, the average component of the residual range in the x direction. It is used to correct the rate of energy absorption, to take into account the finite range of secondaries.

In view of the small contribution of the secondary electrons to the various quantities under investigation (except the energy spectrum) the contribution of the tertiaries will be in turn, much smaller than the secondary. Consequently it was not calculated.

The secondary flux, current and charge are shown by curves II in Figs. 1, 2, and 3, respectively. The total flux, current and charge is shown by curves III of the same figures.

V. THE POINT MONODIRECTIONAL BEAM

The geometry of the problem indicates the use of cylindrical coordinates (r, ϕ, z) for the position variables with the z axis lying along the line of fire, and spherical coordinates $(\vartheta, \Phi + \phi)$ for the direction of momentum; the angle Φ is chosen in a way that $\Phi = 0$ refers to a plane defined by the z axis and the point (r, ϕ, z) . Finally, the magnitude of momentum is given again in terms of the residual track length, $R(t)$. The transport equation in the reduced variables, $r = R_0 \rho$, $z = R_0 x$, $R = R_0 t$, is

Equations (37) are solved chainwise starting from $p = m = 0$. Then one proceeds to $p = 1, m = \pm 1$, and then to $p = 2, m = -2, 0, 2$, etc. The $I_{l,m}^{n,p}(t)$ decrease rapidly with increasing values of p , so only values of $p \leq 4$ were considered.

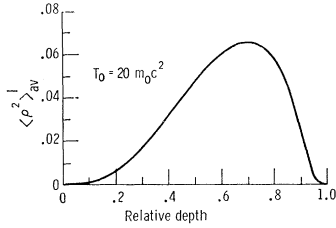


FIG. 9. Point mono-directional beam. The mean-square radial deviation of the flux $\langle \rho^2 \rangle_{av}^I$ as a function of the relative depth, $x = z/R_0$.

The integrals

$$i_{l,m}^{n,p} = \int_0^1 I_{l,m}^{n,p}(t) dt, \tag{38}$$

$$j_{l,m}^{n,p} = \int_0^1 S(t) I_{l,m}^{n,p}(t) dt$$

were obtained. From these moments a variety of quantities can be constructed. Here we report on only two:

(1) The mean-square average of the flux as a function of depth:

$$\langle \rho^2 \rangle_{av}^I = I_{0,0}^{p=2}(x) / I_{0,0}^{p=0}(x). \tag{39}$$

(2) The mean-square average of the rate of energy dissipation:

$$\langle \rho^2 \rangle_{av}^J = J_{0,0}^{p=2}(x) / J_{0,0}^{p=0}(x). \tag{40}$$

The moments of $I_{0,0}^{p=2}$, $J_{0,0}^{p=2}$, plotted on semilog paper against $(n+4)^{1/2}$, indicate that $I_{0,0}^{p=2}(x)$, $J_{0,0}^{p=2}(x)$ behave exponentially for $|1-x| \ll 1$ [see Eq. (23)] and as x^3 for $x \ll 1$, the latter agreeing with the small depth, small-angle approximation.^{25,26}

The functions $I_{0,0}^{p=2}(x)$, $J_{0,0}^{p=2}(x)$ are of the form

$$F(x) = Ax^3(1-x)^{-\gamma} \exp\{-a^2x(1-x)^{-1}\}. \tag{41}$$

The parameters A , γ , a^2 are given in Table V. The $\langle \rho^2 \rangle_{av}^I$, $\langle \rho^2 \rangle_{av}^J$ are plotted in Figs. 9 and 10, respectively. They exhibit a maximum at moderately large depths, decaying to zero as $x \rightarrow 1$. This is expected, since the particles that have arrived near $x = 1$ must have suffered practically no deflections. The quantity $\langle \rho^2 \rangle_{av}^J$, Fig. 10, is compared to the same quantity obtained from Berger's Monte-Carlo calculations for the quantity $F(J, M)$ (Berger's notation), the energy dissipation at various depths as function of lateral position, by calcu-

TABLE V. Values of the parameters in $I_{00}^{p=2}$, $J_{00}^{p=2}$.

T_0	$I_{00}^{p=2}$			$J_{00}^{p=2}$		
	A	γ	a^2	A	γ	a^2
$39m_0c^2$	0.226	-1	0.57	0.188	-1	0.57
$30m_0c^2$	0.344	-1	0.68	0.297	-1	0.68
$20m_0c^2$	0.801	$-\frac{1}{2}$	0.75	0.879	0	0.57

²⁵ B. Rossi and K. Greisen, Rev. Mod. Phys. 13, 240 (1941).

²⁶ H. S. Snyder and W. T. Scott, Phys. Rev. 76, 220 (1949).

lating the sums

$$\sum_M \langle \rho_M^2 \rangle F(J, M) \cong \sum_M \frac{1}{2} (\rho_M^2 + \rho_{M+1}^2) F(J, M).$$

Some error is expected in substituting $\frac{1}{2}(\rho_M^2 + \rho_{M+1}^2)$ for $\langle \rho_M^2 \rangle$, especially for low M values. Agreement at most points is satisfactory.

It is of some interest to write the generalization of Eq. (13):

$$x^2 + \rho^2 \leq (1-t)^2. \tag{42}$$

In particular:

$$\langle x^2(t) \rangle_{av} + \langle \rho^2(t) \rangle_{av} \equiv [I_{0,0}^{2,0}(t) + I_{0,0}^{0,2}(t)] / I_{0,0}^{0,0}(t) \leq (1-t)^2,$$

from which

$$\langle \langle x^2(t) \rangle_{av} \rangle_{av} + \langle \langle \rho^2(t) \rangle_{av} \rangle_{av} \leq \frac{1}{3}.$$

VI. CERTAIN COMMENTS ON THE NUMERICAL CALCULATIONS

The solution of our problem has proceeded along exact analytical lines up to the derivation of a mathematical expression for the quantities $I_{l,n}(t)$ and $I_{l,m}^{n,p}(t)$. The last step, the evaluation of this expression, had to be done by numerical methods. The numerical work proceeded in the following way.

First the rate of ionization and radiation losses was carefully recalculated and checked against calculations of other authors. Next the range was computed by means of

$$R(T) = \int_0^T dT/S(T)$$

and plotted against energy. The result is very nearly a straight line for $T > 2m_0c^2$.

Then the quantities $S_l(t)$ were computed as a function of the kinetic energy T (T is expressed in m_0c^2 units, as usual) and then plotted against the variable t , to obtain $S_l(t)$. The method of derivation of $S_l(t)$ imposes the restriction $\eta l \ll 1$. In m_0c^2 units this becomes:

$$(137)^{-1} l [T(T+2)]^{-1/2} \ll 1.$$

This condition is amply obeyed by all the quantities

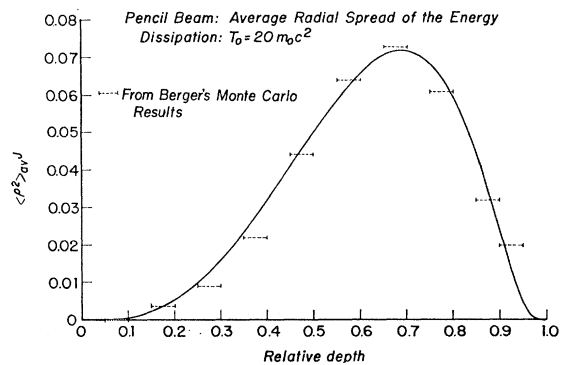


FIG. 10. Point monodirectional beam. The mean-square radial deviation of the rate of energy dissipation $\langle \rho^2 \rangle_{av}^J$ as a function of the relative depth, $x = z/R_0$.

that were calculated. The $S_l(t)$ and $\int_0^t S_l(t)dt$ are increasing with decreasing t , so the $I_{l0}(t)$ are all equal to unity at $t=1$ and decrease monotonically for $t<1$. The rate of decrease becomes faster with higher values of l . The quantity $I_{l0}(t)$ was calculated for all t such that $I_{l0}(t) \geq 10^{-5}$ except for $l=1$, where $I_{l0}(t) \geq 10^{-3}$. Thus, for $T_0=39m_0c^2$ and $l=1$, we have $t_{\text{cutoff}}=0.0002$, $T_{\text{cutoff}}=0.06m_0c^2$, and $\eta l=(48.2)^{-1}$. For $l=10$, we have $t_{\text{cutoff}}=0.3$, $T_{\text{cutoff}}=10.5m_0c^2$ and $\eta l=(156)^{-1}$. The $S_l(t)$ and all subsequent quantities were obtained for a large number of closely spaced values of t , with the aid of a desk calculator. The $I_{ln}(t)$, $I_{l,m^{n,p}}(t)$, $i_{l,n}$, $i_{l,m^{n,p}}$ were calculated by an IBM 7090 computer.

Finally, the construction of the various functions from their moments was done with the aid of a desk calculator and tables of the various standard functions. A computer was not found particularly useful in this situation because of the changing algebraic structure of the trial functions from one trial to the next.

VII. COMPARISON WITH EXPERIMENT

In a comparison with experiment, it is desirable that the experimental conditions closely approximate the theoretical boundary conditions. For comparison with the plane parallel beam results, a wide, monodirectional, monoenergetic beam of uniform cross-sectional intensity is desired. The dimensions of the medium should be larger than the maximum electronic range. It is difficult to satisfy all these requirements experimentally. The experimental requirements are made less stringent when the principle of reciprocity between source and detector is taken into account; for example, data on the plane parallel beam of a given finite (or infinite) size can be obtained from information on a narrow (pencil) beam: an integration over the pencil sources constituting the finite (or infinite) beam is equivalent to an integration over the appropriate range of ρ , at the depth of observation, of the results of a single pencil beam. The nonuniform cross-sectional intensity of the finite beam can also be taken into account by use of an appropriate weight factor in the integration over ρ . However, to the author's knowledge, there are no experimental data at points off the central axis.

If the experimental beam is not initially monochromatic but possesses a known spectrum, comparison with theory is still possible by appropriate superposition of theoretical curves with various T_0 .

However, the methods of obtaining an electron beam of a given cross-sectional area introduce into the beam certain undesirable features. In order to obtain a wide beam of reasonably uniform cross-sectional intensity, the emergent betatron beam which is very narrow is scattered by thin foils of aluminum and/or lead. This changes the monochromatic nature of the beam by creating a spectrum of electrons with less than the maximum energy. It also produces a small but noticeable amount of bremsstrahlung x rays (a 20-MeV electron traversing a foil of 0.027 in. of Al and 0.010 in.

of Pb loses an average of 0.86 MeV to x rays; this is to be compared with the 1.6-MeV bremsstrahlung loss in the water medium itself) which tends to extend the deep penetration tail of the distribution.

The scattering foils also destroy the monodirectional nature of the beam. Without the foils the beam already has divergent properties and is contained in a cone of half-angle of about 5° . The foils strongly increase this divergence. Even though the beam is subsequently collimated by a Lucite cone of the desired cross section, the beam emerging from the cone still contains many strongly divergent components. The result is that the maximum of $I_0(x)$ will be shifted towards lesser depths and will display a less steep decay after the maximum. The functions $I_1(x)$ will also display an earlier and less steep decay, which means that

$$Q(x) = -dI_1(x)/dx$$

will exhibit a broader maximum. This is experimentally observed.

The production of bremsstrahlung has a similar effect of decreasing the steepness of the curves at large x and of extending the tails beyond the maximum electronic range. The statistical nature of radiative energy losses means that there will be some electrons that have suffered more losses or fewer losses than the average. Those which lose less by this process will be able to travel more and thus slightly extend the deep penetration tail of the distribution.

A set of experiments was performed at Memorial Hospital to obtain the quantity $Q(x)$ and compare it with theory. The experimental points are shown in Fig. 3.²⁷ As already anticipated, the maximum is broader, but still very near the theoretically predicted depth. The experimental data also confirm the existence of a region of positive charge at small depths.

The existence of a rather narrow region of charge accumulation at relatively large depths has also been observed in dielectrics by various authors.²⁸

A set of current distribution (transmission) curves was calculated by Leiss⁹ by Monte-Carlo methods, taking into account ionization, scattering, and radiation straggling. The medium was carbon. The results are closely similar to ours; the effect of radiation straggling, while noticeable at 20 MeV, is again seen to produce simply a small stretching of the curve toward larger depths.

Experimental current and charge distributions have been obtained in Plexiglas and aluminum for low-energy electrons (2–3 MeV).²⁹ It is seen that qualitatively the curves are similar to ours. For the low-energy beams considered, one would expect the current to decrease

²⁷ J. S. Laughlin, H. Astarita, J. Reisinger, and M. Danzker, presented at the 48th annual meeting of the Radiological Society of North America, 1958 (to be published).

²⁸ B. Gross, Phys. Rev. **107**, 368 (1957); J. Polymer Sci. **27**, 137 (1958).

²⁹ J. G. Trump, K. A. Wright, and A. M. Clarke, J. Appl. Phys. **21**, 345 (1950).

much faster with depth, and the region of maximum charge accumulation to be at a smaller relative depth than ours. This is indeed what was observed. However, the region of positive charge for $x \ll 1$ was passed unnoticed, probably because at these energies it is confined to a very thin slice near $x=0$, and it is thus difficult to detect experimentally.

A set of Monte-Carlo calculations were performed recently by Perkins⁴ to obtain transmission curves in aluminum for electrons of energies between 0.4 and 4.0 MeV. Although there can be no quantitative comparison between these results and ours, Fig. 2, the curves are qualitatively similar.

ACKNOWLEDGMENTS

The author is indebted to Dr. John S. Laughlin, Division of Biophysics, Sloan-Kettering Institute, for suggesting the general topic and for many useful discussions. The author expresses his gratitude to Professor W. H. Furry, Harvard University, for invaluable suggestions, comments, and encouragement in his capacity as thesis adviser. The valuable aid of William Siler and Frank Ritter in programming parts of the problem for the IBM 7090 computer, and the cooperation of Kenneth King and the Watson Scientific Computing Laboratories and of the The Bendix Computer, Inc., computer group are deeply appreciated.

Nuclear Magnetic Resonance Studies of Some Materials Containing Divalent Europium*

E. L. BOYD†

IBM Watson Research Center, Yorktown Heights, New York

(Received 8 November 1965)

This paper reports the results of a low-temperature NMR experiment on Eu^{153} in EuO . The data, which are assumed to be linear with magnetization, are compared with calculated values using spin-wave theory. Values of $J_1/k_b = 0.750 \pm 0.0025^\circ\text{K}$ and $J_2/k_b = -0.0975 \pm 0.004^\circ\text{K}$ are found to give a good description of EuO . This paper also reports the results of NMR studies of the ligands F^{19} and Cs^{137} in EuF_2 and CsEuF_4 . These experiments indicate that there is a reversal in sign of the unpaired spin density of the europium ion. The same results are obtained with europium-bearing glasses. This effect is discussed in terms of the Freeman-Watson model of Gd^{3+} and in terms of a virtual $5d$ state in Eu^{2+} .

INTRODUCTION

THIS paper presents the experimental results of some nuclear resonance experiments on the Eu^{153} resonance in ferromagnetic EuO and on the Cs^{133} , F^{19} , and B^{11} resonance in some paramagnetic Eu salts and glasses. Since the two experimental techniques are different and since the results given are in a limited sense different they will be discussed separately in the paper. On a more general level, however, the NMR experiment, whether done on the magnetic ion in a ferromagnet or on a ligand in a paramagnet, always measures the local field at the nucleus involved. This local field differs from any external field by the amount of electron-spin polarization at the nuclear site. The electron-spin polarization results ultimately from the amount of unpaired spin on the magnetic ion (the $4f$ electrons of the europium ion in this case). The spontaneous magnetization of a compound results from a favorable alignment of this unpaired spin distribution throughout the crystal. In the magnetic metals the

conduction electrons are slightly polarized and bear the magnetic information from atom to atom. In the insulators, such as EuO , there is a polarization of the core which results in the large hyperfine interaction and a polarization of the valence electrons which results in the exchange and thereby the magnetic alignment. By probing with nuclear resonance one learns something about the spatial variation of this polarization of the nonmagnetic electrons.

NUCLEAR MAGNETIC RESONANCE IN FERROMAGNETIC EuO

Uriano and Streever¹ have found the nuclear resonance of Eu^{153} in EuO at 4°K by using the spin-echo technique. They report echoes over a 20 Mc/sec wide frequency range from 125 to 145 Mc/sec with a maximum intensity at a frequency of 138 Mc/sec. The study of this resonance by cw techniques is reported in this paper.

The most striking difference between the two experiments is the cw linewidth which is ≈ 80 kc/sec at 4.2°K . Uriano reports values for T_1 (9×10^{-3} sec) and T_2 (40×10^{-6} sec) obtained from the spin-echo experiment which

¹ G. A. Uriano and R. L. Streever, *Phys. Letters* **17**, 205 (1965).

* Work supported in part by the U. S. Air Force Office of Scientific Research under Contract No. AF 49(638)-1230.

† Present address: IBM Systems Development Division, Poughkeepsie, New York.